Structural and functional impairment of endocytic pathways by retinitis pigmentosa mutant rhodopsin-arrestin complexes

Jen-Zen Chuang,[1] Carrie Vega,[1] Wenjin Jun,[1] and Ching-Hwa Sung[1,2]

[1]Department of Ophthalmology, The Margaret M. Dyson Research Institute, and [2]Department of Cell and Development Biology, Weill Medical College of Cornell University, New York, New York, USA.

Retinitis pigmentosa (RP) is a clinically and genetically heterogeneous degenerative eye disease. Mutations at Arg135 of rhodopsin are associated with a severe form of autosomal dominant RP. This report presents evidence that Arg135 mutant rhodopsins (e.g., R135L, R135G, and R135W) are hyperphosphorylated and bind with high affinity to visual arrestin. Mutant rhodopsin recruits the cytosolic arrestin to the plasma membrane, and the rhodopsin-arrestin complex is internalized into the endocytic pathway. Furthermore, the rhodopsin-arrestin complexes alter the morphology of endosomal compartments and severely damage receptor-mediated endocytic functions. The biochemical and cellular defects of Arg135 mutant rhodopsins are distinct from those previously described for class I and class II RP mutations, and, hence, we propose that they be named class III. Impaired endocytic activity may underlie the pathogenesis of RP caused by class III rhodopsin mutations.

Introduction

Retinitis pigmentosa (RP) is a progressive retinal degenerative disease. Nearly 100 mutations of the rhodopsin gene have been identified in patients with autosomal dominant RP, and these mutations account for approximately 25% of autosomal dominant RP. The study of mutant rhodopsins suggested that some RP mutations impair protein folding, 11-*cis* retinal chromophore binding, G-protein coupling/activation, and/or cellular trafficking of the rhodopsin protein (1–4). On the basis of their biochemical defects, RP mutant rhodopsins have been classified into two groups: class I and class II (4, 5). Class I mutants resemble WT rhodopsin, form functional photopigment upon 11-*cis* retinal reconstitution, and exhibit plasma membrane (PM) distribution when expressed in human embryonic kidney (HEK) cells. By contrast, class II mutants are defective in 11-*cis* retinal assembly and are either completely or partially retained in the endoplasmic reticulum.

Rhodopsin, the visual pigment of rod photoreceptors, is a prototypic G-protein–coupled receptor (GPCR). In vertebrates, light illumination results in the isomerization of chromophore, which induces the activation of rhodopsin and the downstream G-protein (transducin) cascade. The desensitization of rhodopsin is mediated by phosphorylation of rhodopsin kinase (RK), which induces the uncoupling of heterotrimeric G-protein complexes and subsequent binding of visual arrestin (v-arr). Thus, v-arr binding sterically blocks and rapidly uncouples the rhodopsin-transduction interactions. Sequestration (internalization of the receptor from the cell surface) has been described for many GPCRs as an additional mechanism to deactivate surface signaling, but such a pathway has not been described for mammalian rhodopsins. Interestingly, recent work carried out in *Drosophila* suggests that stable complexes form between rhodopsins and mutant v-arr. These complexes undergo endocytosis, and this process may be the key element responsible for the photoreceptor death in the light-dependent retinal degeneration models in the fly (6, 7).

Endocytosis, a process that removes macromolecules and their cognate receptors from the cell surface by internalization, contributes to distinct cellular functions such as nutrient uptake, ion transport, and signaling deactivation. The endocytosed molecules are first delivered to and sorted at early endosomes before their further targeting to either the recycling pathway or the degradation pathway. In the recycling pathway, recycling proteins such as transferrin (Tf) are recycled back to the cell surface. In the degradation pathway, ligands such as LDL move to the lysosomes via late endosomes (8). Although the molecular differences between the various endocytic compartments are blurred, early endosomes, recycling endosomes, and late endosomes are considered to be distinct compartments, each with different lumenal pH. The formation and maintenance of the endocytic architectural framework, which rely on well-regulated, highly dynamic interplays between these membrane domains, are essential for proper endocytic functions (9).

In this study, we show that an RP mutant rhodopsin with a substitution at Arg135 was hyperphosphorylated and constitutively internalized in HEK cells. A representative Arg135 mutant, R135L, exhibited constitutional phosphorylation and a high affinity for binding to v-arr in the absence of chromophore. R135L recruited and translocated cytosolic v-arr to the PM and the endocytic compartments. Similarly, photoreceptors that ectopically expressed R135L also exhibited mislocalization of v-arr. Finally, aberrant membrane compartments that contained a mixture of early, recycling, and late endosomes were formed, and receptor-mediated endocytic activity was impaired in cells expressing R135L/v-arr complexes.

Results

R135L mutant rhodopsins are hyperphosphorylated and constitutively internalized. Several mutant bovine rhodopsins with amino acid

Nonstandard abbreviations used: chicken -actin promoter with CMV enhancer (pCAG); 3,3′-diotadecylindocarbocyanine (DiI); early endosome antigen 1 (EEA1); G-protein–coupled receptor (GPCR); GPCR kinase (GRK); human embryonic kidney (HEK); internal ribosome entry site (IRES); plasma membrane (PM); retinitis pigmentosa (RP); rhodopsin kinase (RK); transferrin (Tf); transferrin receptor (TfR); visual arrestin (v-arr).

Conflict of interest: The authors have declared that no conflict of interest exists.

Citation for this article: *J. Clin. Invest.* **114**:131–140 (2004). doi:10.1172/JCI200421136.

changes at Arg135 have been shown to exhibit higher affinity to RK and v-arr in vitro (10). Three known human autosomal dominant RP-associated rhodopsin missense mutations occur at Arg135 (R135G, R135L, and R135W) (11, 12). Our intention, therefore, was to examine the interaction between v-arr and human Arg135 mutants in transfected HEK cells. Our preliminary experiments revealed that all three Arg135 mutants behaved similarly. In this report, the R135L mutant is shown as a representative.

Consistent with previous reports (4), WT rhodopsin predominantly accumulated on the PM of transfected HEK cells (Figure 1A). However, the R135L mutant rhodopsin displayed varied expression patterns in transfected cells. When the expression level was high, the mutant protein was detected on endoplasmic reticulum and nuclear membranes (data not shown). However, in cells that expressed a modest level of R135L, the distribution of rhodopsin appeared to be on both the cell surface and the intracellular vesicles throughout the cytoplasm (Figure 1B). To test whether these vesicles represented various endocytic compartments, we performed bioassays in which the fluorescence-conjugated ligands (e.g., Tf and dextran) internalized and traveled through various endocytic compartments (e.g., early, recycling, and late endosomes) inside cells, depending on the incubation time and the type of ligand. These assays allow detection of endocytic compartments without perturbing the morphology or function of endosomes (13). In these assays, some R135L signals were found in early endosomes where Alexa 594–Tf was primarily distributed after a 5-minute uptake (Figure 1, C–E). This finding was consistent with the partially overlapped colocalization between the R135L signal and the immunolabeling of the early endosomal markers, early endosome antigen 1 (EEA1) and Rab5 (data not shown). The R135L signals were also present in the perinuclear recycling endosomes, where the Tf was primarily distributed after a 2-minute uptake followed by a 28-minute chase (Figure 1, F–H). Finally, R135L signals were detected on late endosomes/lysosomes, which were labeled by the internalized rhodamine-dextran after a 2-hour loading (Figure 1, I–K). The distribution of R135L to the endosomes and lysosomes was consistently observed in HEK cells stably expressing this mutant protein (data not shown). The expression patterns of R135L suggested that the mutant rhodopsins were constantly internalized from the cell surfaces and that they were either sent back to the cell surface via recycling endosomes or delivered for lysosomal degradation.

To assess whether the constitutive internalization of R135L was possibly caused by the hyperphosphorylation of mutant rhodopsins, we sought to determine the phosphorylation state of the R135L mutant protein expressed in HEK cells. Cells cotransfected with WT rhodopsin and RK served as positive control cells, because overexpressed GPCR kinases (GRK) has been reported to phosphorylate GPCRs in cell cultures, even in the absence of ligand. As noted previously (4, 14), rhodopsin expressed in HEK cells appears as a heterogeneous species of protein bands on SDS-PAGE and represents monomers, dimers, and higher-

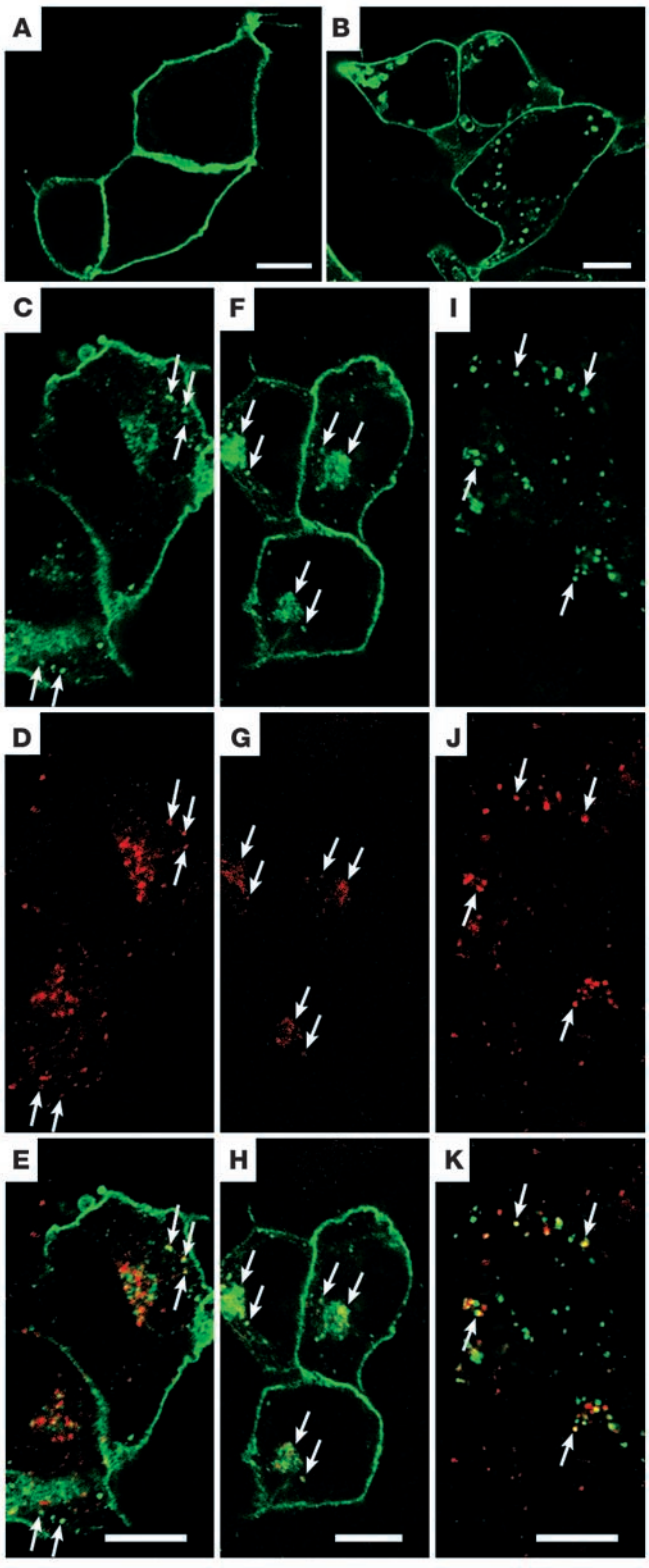

Figure 1
Confocal images of WT and mutant rhodopsins expressed in HEK cells. (**A** and **B**) Fixed HEK cells transfected with WT (**A**) or R135L (**B**) rhodopsin were incubated with anti–rhodopsin mAb B6-30 and detected by Alexa 488 secondary antibodies. (**C**–**K**) HEK cells transfected with R135L were incubated with Alexa 594–Tf for 5 minutes to label early endosomes (**C**–**E**); incubated with Alexa 594–Tf for 2 minutes followed by a 28-minute chase to label recycling endosomes (**F**–**H**); or incubated with rhodamine-labeled dextran for 2 hours to label late endosomes/lysosomes (**I**–**K**). Cells were then fixed and permeabilized for rhodopsin immunostaining (green). Rhodopsin immunoreactivity colocalized with the internalized Tf or dextran is marked by arrows, and merge images are shown in **E**, **H**, and **K**. Scale bars: 10 μm.

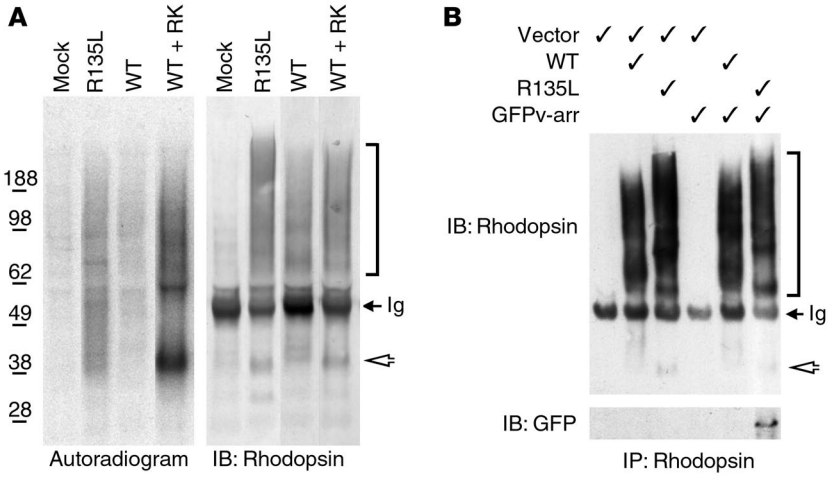

Figure 2

Phosphorylation and v-arr association of R135L rhodopsin in HEK cells. (**A**) Immunoprecipitated rhodopsin, obtained from transfected cells that had been metabolically labeled with [^{32}P] orthophosphate, were subjected to SDS-PAGE and either autoradiographed (left) or immunoblotted (right). (**B**) Rhodopsin immunoprecipitates obtained from cells transfected with pRK5 vector, rhodopsin and/or GFPv-arr (as indicated) were separated by SDS-PAGE and immunoblotted with either anti-rhodopsin Ab (top) or anti-GFP Ab (bottom) (GFPv-arr: ~75 kDa). Rhodopsin expressed in tissue culture is heterogeneously glycosylated and prone to forming higher-order aggregates (2, 5), which accounts for the broadened bands on SDS-PAGE. Arrowheads point to the rhodopsin monomer (~40 kDa), and the brackets indicate the heterogeneous species of oligomerized rhodopsins. The electrophoretic patterns of R135L rhodopsins were distinct from those of WT rhodopsins, perhaps because of the conformation changes caused by the mutation. Some 50-kDa Ig heavy chains were reactive with the secondary antibodies (arrows). Results are representative of three experiments. IB, immunoblot; IP, immunoprecipitate.

order oligomers, each of which is heterogeneously glycosylated (Figure 2A, right panel). Autoradiograms of immunoprecipitated rhodopsin showed that little or no phosphorylated rhodopsin was detected in lysates obtained from cells singly transfected with WT rhodopsin or from mock-transfected cells (Figure 2A, left panel). As expected, the WT rhodopsin was highly phosphorylated when it was coexpressed with RK. In addition, a significant level of phosphorylated R135L rhodopsin was also detected. These results suggested that the R135L was phosphorylated by the endogenous GRK and was endocytosed into the cells like an activated GPCR.

R135L mutant rhodopsin is stably associated with v-arr. To measure the association between rhodopsin and v-arr, we examined the ability of v-arr to be coprecipitated by anti-rhodopsin Ab from lysates of HEK cells that coexpressed v-arr and rhodopsin. GFPv-arr was used in these experiments because GFPβ-arrestin fusion proteins are reportedly useful in studying the functional interaction between arrestin and GPCRs, and they can be directly visualized by microscopy (15, 16). Anti-rhodopsin mAb efficiently precipitated both WT and R135L mutant rhodopsin (Figure 2B). However, GFPv-arr could only be coprecipitated by the R135L mutant rhodopsin, not by WT rhodopsin. Consistently, the converse immunoprecipitation experiments showed that R135L, but not WT rhodopsin, was coimmunoprecipitated with GFPv-arr by anti-GFP Ab (data not shown).

To assess the functional interaction between GFPv-arr and R135L mutant rhodopsin, we examined their subcellular distributions in transfected cells. As expected, GFPv-arr was distributed in the cytosol throughout the cells (data not shown). In cells that coexpressed WT rhodopsin and GFPv-arr, rhodopsin was distributed on the PM, whereas GFPv-arr remained in the cytosol (Figure 3, A–C). By contrast, in cells that coexpressed R135L and GFPv-arr, GFP signals were primarily detected on the cell surface and intracellular vesicular structures (Figure 3, D–F). The GFP signals, both on the cell surface and in the intracellular vesicular compartments, were largely colocalized with R135L mutant rhodopsin signals. The noncytosolic distribution of GFPv-arr appeared to depend on the expression level of R135L rhodopsin: residual cytosolic GFPv-arr was detected in cells that expressed a low level of mutant rhodopsin (Figure 3, D–F, open arrows). Most cells in 18-hour to 24-hour cultures contained a single prominent GFP$^+$ structure near the cell center (Figure 3, D–F, arrowhead). Occasionally, these structures appeared to be a cluster of small vesicles with clear boundaries. However, these structures were often amorphous or opaque looking (see Figure 6I). A confocal three-dimensional projection revealed that the perinuclear GFP$^+$ structure was cup shaped, which is consistent with the horseshoe appearance seen in some planes (see Figures 5A and 6I). No such structures were found in cells that coexpressed GFP and R135L (data not shown). Modifying the plasmid levels for transfection from 1:1 to 5:1 for R135L and GFPv-arr had no effect on the results (data not shown)

In 48-hour cultures, most cells that carried the perinuclear GFP$^+$ cup-shaped structures appeared unhealthy; they possessed a rounded-up cell shape and abnormal nuclei (Supplemental Figure 1, A and B; supplemental material available at http://www.jci.org/cgi/content/full/114/1/131/DC1). These signs both indicate cytotoxicity. In contrast, the cell and nuclear morphologies of the cells that overexpressed WT rhodopsin/GFPv-arr at this time point remained largely normal (Supplemental Figure 1, C and D). The pathology of HEK cells that expressed R135L/GFPv-arr was further supported by the observation that significantly higher death, determined by Annexin V affinity assay (17), was found in cells that expressed R135L/GFPv-arr compared with cells that expressed either WT rhodopsin/GFPv-arr, GFPv-arr, or GFP alone (Supplemental Table 1).

Typical class I (e.g., Q344ter) (data not shown) and class II (e.g., P23H) (Figure 3, G–I) mutant rhodopsins did not codistribute with GFPv-arr, and no GFP$^+$ perinuclear structures formed in cells that coexpress GFPv-arr and either of these mutant rhodopsins. Misfolded P23H mutants have been reported to induce the formation of aggresome, a centrosomal spherical structure that acts as a repository for misfolded proteins (14). However, we found no enrichment of GFP signal in the aggresomes occasionally seen in the P23H/GFPv-arr cotransfected cells (Figure 3, G–I, open arrows). In addition, the morphological characteristics of aggresomes were distinct from that of the cup-shaped structures caused by R135L/v-arr complexes.

Bidirectional vesicular trafficking between endosomal compartments and the trans-Golgi network has been reported (18, 19). To be certain that the intracellular R135L signals were derived from the cell surface via endocytosis, we incubated live HEK cells that

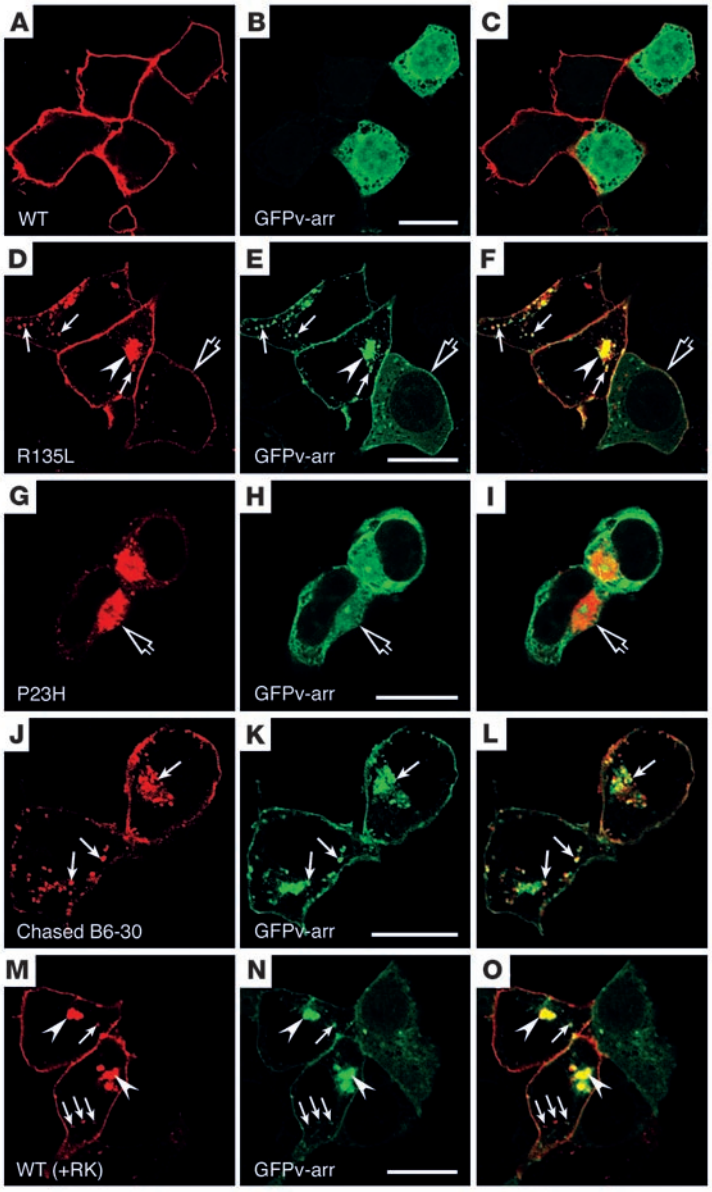

Figure 3
Subcellular distribution and trafficking of rhodopsin in HEK cells cotransfected with GFPv-arr. (**A**–**I**) Cells double transfected with GFPv-arr and either WT rhodopsin (**A**–**C**), R135L (**D**–**F**), or P23H (**G**–**I**) were immunolabeled for rhodopsin (red), and GFPv-arr was directly visualized by its GFP fluorescence. In **D**–**F**, some cells expressed low levels of R135L and contained both surface and cytosolic GFP signals (open arrows); the vesicular structures near the cell periphery (arrows) and the perinuclear structure (arrowheads) contain both the R135L and the GFPv-arr. In **G**–**I**, the P23H mutant–induced aggresomes (open arrows) are not enriched for GFPv-arr. (**J**–**L**) Live, R135L/GFPv-arr–transfected cells were incubated with mAb B6-30 at 4°C, followed by a 1-hour, 37°C chase. The cells were fixed and permeabilized, and the internalized rhodopsin was detected by the labeling of Alexa 594–anti-mouse Ab (red). Internalized surface rhodopsins appeared on GFPv-arr$^+$ vesicle and perinuclear compartments (arrows). (**M**–**O**) Cells triple-transfected with WT-rhodopsin, RK, and GFPv-arr were fixed, permeabilized, and either immunolabeled with mAb B6-30 followed by Alexa 594–anti-mouse Ab (**M**) or directly visualized by GFP signals (**N**). Phosphorylated WT rhodopsin was colocalized with GFPv-arr on the vesicles underneath PM (arrows) and the perinuclear compartments (arrowheads). A GFPv-arr–singly-transfected neighboring cell exhibited cytosolic green fluorescence. Scale bars: 20 μm.

expressed R135L/GFPv-arr with anti–rhodopsin N-terminus mAb B6-30 at 4°C and chased at 37°C for various time periods. Cells were then fixed and incubated with Alexa 594–conjugated secondary Ab to visualize the rhodopsin derived from the cell surfaces. At the 30-minute chase time point, the immunolabeling of internalized rhodopsin was largely correlated with the peripheral GFP$^+$ early endosomes (data not shown). After a 1-hour chase, a significant amount of rhodopsin signals appeared at the GFP$^+$ intracellular vesicles and perinuclear compartment (Figure 3, J–L, arrows). These results suggested that surface-derived R135L cotrafficked with GFPv-arr as a protein complex and these protein complexes transited through the early endosomes before being targeted to the cup-shaped perinuclear compartments.

In trying to determine the physiological relevance of rhodopsin endocytosis, we questioned whether hyperphosphorylation also leads to the endocytosis of WT rhodopsin. On the basis of the above results, we predicted that WT rhodopsin phosphorylated by RK should resemble the R135L mutant and exhibit constitutive internalization. Indeed, we found that WT rhodopsin in cells cotransfected with RK was distributed on both the PM and intracellular endosomal/lysosomal compartments and was indistinguishable from that of R135L mutant rhodopsin (data not shown). Moreover, the PM and vesicular GFPv-arr distribution (Figure 3N, arrows and arrowheads) in cells that coexpressed RK and WT rhodopsin (Figure 3M) was indistinguishable from that in R135L/GFPv-arr–transfected cells. These results indicated that the hyperphosphorylated rhodopsins were capable of binding and entering cells together in a complex with v-arr.

Mislocalization of v-arr in transfected rods expressing R135L mutant rhodopsin. To corroborate our in vitro studies, we sought to examine whether the R135L mutant rhodopsin also modulated the v-arr distribution in vivo. No transgenic mouse line that expressed the R135L mutant has been generated at the present time. We, thus, investigated these questions by making use of a recently developed ectopic retinal expression system (20). In these experiments, a bicistronic expression vector, chicken -actin promoter with CMV enhancer–rhodopsin-IRES-GFP (pCAG-rhodopsin-IRES-GFP), which drives both rhodopsin and GFP expression in the same transfected cells, was injected into the subretinal space of neonatal rat, followed by electroporation (Figure 4, A and B). Transfected retinas were harvested and processed for immunostaining at postnatal week 3 to 4, when retinas reach maturation. As expected (20), most transfected GFP-positive retinal cells were photoreceptors. Consistent with previous reports (20, 21), the GFP signal in transfected rods was uniformly distributed throughout the cells, and somewhat lower signal was found in the outer segment (Figure 4, D, F, and H). By contrast, transfected WT rhodopsin was primarily and specifically targeted to the outer segment; very little or no signal was found in the rest of the cell bodies (Figure 4C). The WT rhodopsin was detected by mAb 3A6, which specifically recognizes exogenously introduced

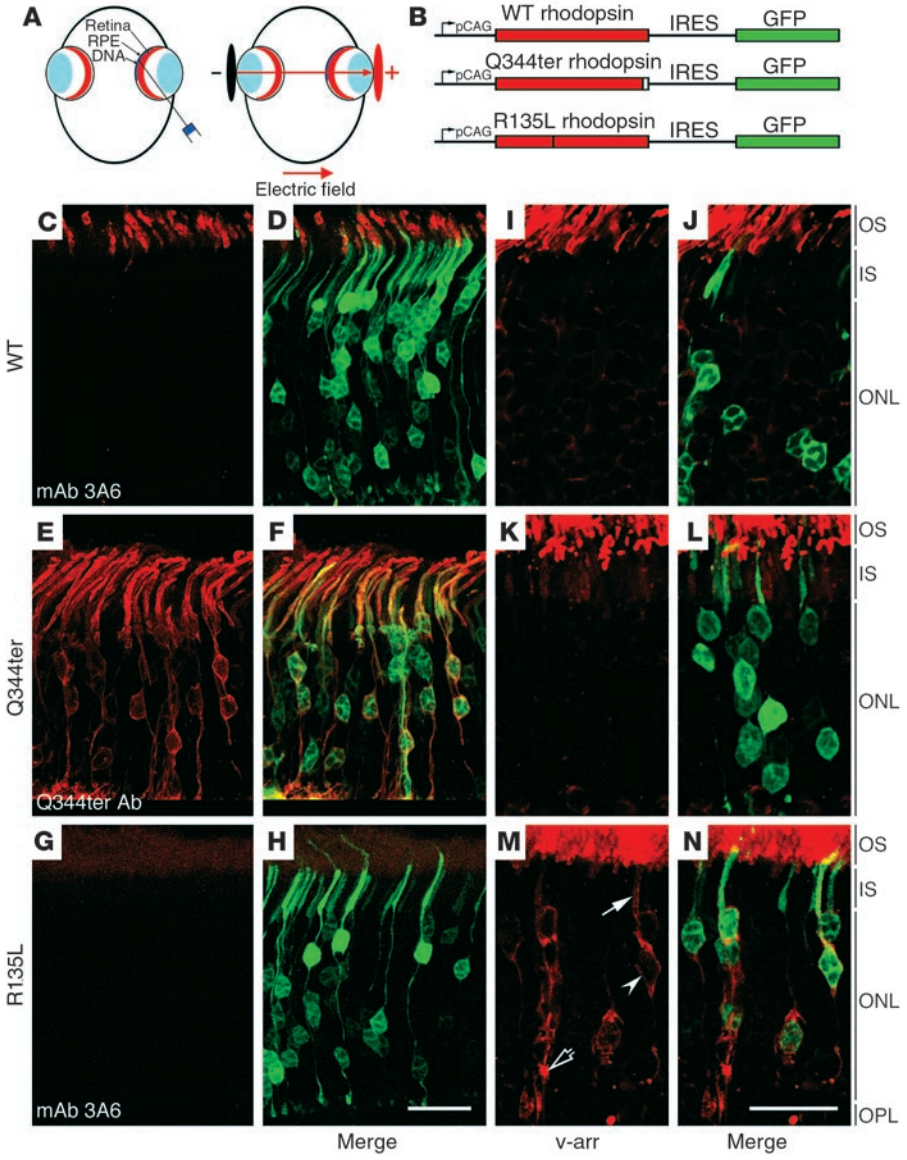

Figure 4
Endogenous v-arr was mislocalized in rodent rods that expressed R135L but not WT or Q344ter rhodopsin. (**A**) The schematic illustration shows the in vivo electroporation technique. Plasmid is injected into the subretinal space followed by electroporation. Tweezer-type electrodes are placed across the eye, with the anode facing the cornea. (**B**) A schematic illustration of the bicistronic expression vector pCAG-rhodopsin-IRES-GFP. These vectors permit both rhodopsin and GFP to be translated from a single mRNA and simultaneously expressed in the transfected cells. (**C**–**H**) Retinas were transfected with either pCAG-WT-IRES-GFP (**C** and **D**), pCAG-Q344ter-IRES-GFP (**E** and **F**), or pCAG-R135L-IRES-GFP (**G** and **H**). These retinas were immunolabeled with the antibodies indicated, followed by Alexa 594–conjugated secondary antibodies. Representative optical images of photoreceptor layer show transfected rhodopsin immunolabeling (**C**, **E**, and **G**). The GFP signals were directly visualized and are shown in the merge images in (**D**, **F**, and **H**). Note that mAb 3A6 effectively detected the WT but not the R135L mutant in transfected cells. (**I**–**N**) Retina sections prepared from eyes transfected with pCAG-WT-IRES-GFP (**I** and **J**), pCAG-Q344ter-IRES-GFP (**K** and **L**), and pCAG-R135L-GFP (**M** and **N**) were immunolabeled with anti–v-arr antibody (red). Representative confocal images of v-arr labeling (**I**, **K**, and **M**) and merge views with GFP^+- transfected cells are shown (**J**, **L**, and **N**). The PM (arrow and arrowhead) and the intracellular vacuole accumulation of v-arr (open arrow) are marked. OS, outer segment; IS, inner segment; ONL, outer nuclear layer; OPL, outer plexiform layer. Scale bars: 20 μm.

human rhodopsin but not rodent rhodopsin (22). These results suggested that rhodopsin delivered by the transfection procedure was properly targeted.

Furthermore, the transfected class I mutant rhodopsin Q344ter, recognized by an anti-Q344ter Ab (23), was not restricted to the outer segment, but instead was present throughout the PM of the entire photoreceptors (Figure 4E). The expression pattern of Q344ter in transfected rods was indistinguishable from that of the same mutant protein expressed in transgenic photoreceptors (23). Consistent with the transgenic results (23), both the WT and the Q344ter mutant rhodopsins had no effect on the proper outer-segment targeting of endogenous rhodopsin (data not shown). Together, the above results suggested that this gene delivery method led to conclusions similar to those obtained by conventional transgenic mouse studies.

We observed that, although HEK cells singly transfected with R135L can be recognized by mAb 3A6 (data not shown), this Ab failed to detect R135L when it was coexpressed with GFPv-arr (Supplemental Figure 2, C and D). By contrast, mAb 3A6 recognized WT rhodopsin even when it was coexpressed with GFPv-arr (Supplemental Figure 2, A and B). The best explanation for these observations is that the constitutive binding of v-arr to the R135L mutant either blocked or modified the mAb 3A6 epitope, which is localized at rhodopsin's C-terminus (24). In transfected rods, the R135L mutant proteins were nicely labeled by the anti–N-terminus mAb B6-30 (data not shown) but not by mAb 3A6 (Figure 4G), which hints that the ectopically expressed R135L was also constitutively bound by the endogenous v-arr in vivo.

The subcellular distribution of endogenous v-arr was examined in photoreceptors that ectopically expressed either WT, Q344ter, or R135L by anti–v-arr Ab immunolabeling (Figure 4, I, K, and M). In these experiments, the bicistronic GFP expression was used to identify the transfected cells, and the animals were harvested under normal lighting. As expected, the v-arr immunoreactivity was predominantly detected in the outer segment of the control and untransfected photoreceptors (Figure 4, I and J), and low-

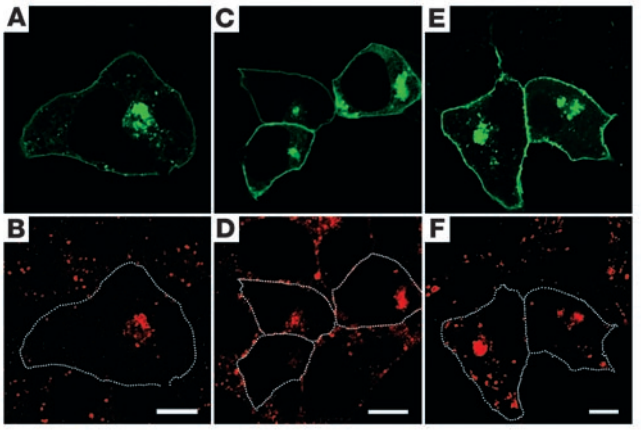

Figure 5
Aberrant endosomal organization caused by R135L/GFPv-arr. Fixed, transfected cells were incubated with mAb's that recognized early endosome marker EEA1 (**A** and **B**), early/recycling endosome marker TfR (**C** and **D**), and late endosome/lysosome marker lysosomal-associated membrane protein 1 (LAMP1) (**E** and **F**), followed by Alexa 594–conjugated anti-mouse Ab. GFP signals were used to directly visualize the GFPv-arr. The transfected cells are encircled in **B**, **D**, and **F** to show the cell margins. Although EEA1, TfR, and LAMP1 signals were dispersed in nontransfected cells, their signals were predominantly concentrated in the GFP$^+$ perinuclear structures in the R135L/GFPv-arr–transfected cells. Scale bars: 10 μm.

level, cytosolic v-arr signal was seen in the rest of cell bodies. The subcellular distribution of v-arr was not affected by the presence of either WT (Figure 4, I and J) or Q344ter mutant rhodopsin (Figure 4, K and L). In sharp contrast, most R135L-transfected rods had significant v-arr accumulated in the cell body: the v-arr was distributed on both the PM of the inner segment and the cell body (Figure 4M, arrow and arrowhead, respectively). Furthermore, prominent perinuclear labeling of v-arr was frequently seen in the R135L-transfected photoreceptors (Figure 4M, open arrow).

Accumulated intracellular R135L rhodopsin–v-arrestin complexes impair the morphologies and functions of endocytic compartments. During the study in HEK cells, we observed that the labeling patterns of endosomal compartments, but not the Golgi apparatus (data not shown), were markedly different between cells carrying R135L/GFPv-arr and neighboring untransfected cells (Figure 5). In the untransfected cells, early endosomes (Figure 5B), early/recycling endosomes (Figure 5D), and late endosome/lysosomes (Figure 5F) were distributed throughout the cytoplasm. In contrast, in the R135L/GFPv-arr–transfected cells, most of these vesicles were concentrated within or near the GFP$^+$ perinuclear structures. For example, the labeling of EEA1 (Figure 5B) and Tf receptor (TfR) (Figure 5D), markers for early endosomes and early/recycling endosomes, respectively, was primarily coincident with the perinuclear GFP$^+$ signals. Nearly no additional immunolabeling was detectable in the remainder of the cytoplasm in cells that expressed high levels of R135L/GFPv-arr. A large subset of immunoreactivity derived from the labeling of lysosomal-associated membrane protein 1 (LAMP1), a molecule present on both late endosomes and lysosomes (9), was also coincident with the GFP signal. However, additional lysosome-like structures remained

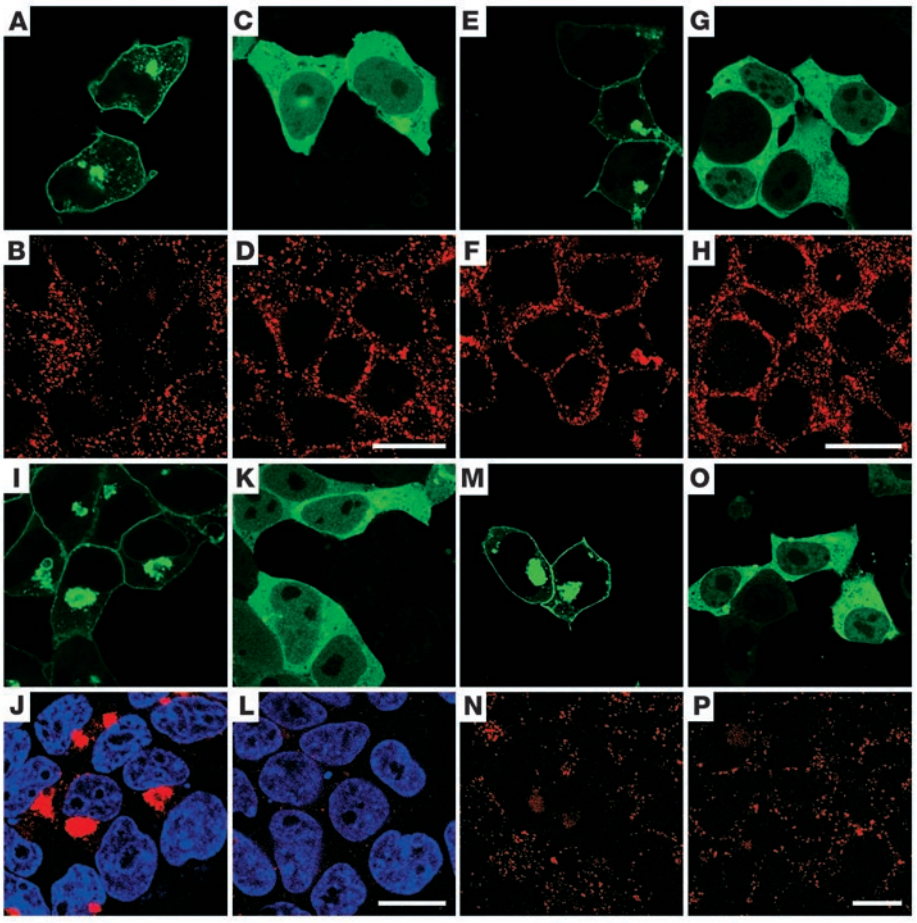

Figure 6
The altered endocytic activity of Tf and LDL in cells that expressed R135L/v-arr. Cells transfected with R135L/GFPv-arr (**A** and **B**, **E** and **F**, **I** and **J**, **M** and **N**) and WT rhodopsin/GFPv-arr (**C** and **D**, **G** and **H**, **K** and **L**, **O** and **P**) were incubated with Alexa 594–conjugated Tf at 37°C for 5 minutes (**A** and **B**, **C** and **D**), for 2 hours (**E** and **F**, **G** and **H**), or for 2 hours plus a 30-minute chase (**I** and **J**, **K** and **L**) before fixation and visualization. Alternatively, cells were treated with DiI-LDL for 2 minutes followed by a 28-minute chase before the fixation (**M** and **N**, **O** and **P**). Confocal images of GFPv-arr (green) and internalized Tf (red) or LDL (red) are shown. In **J** and **L**, the DAPI nuclear labeling demonstrated that the nontransfected cells (in **J** and **L**) and WT/GFPv-arr–transfected cells (in **L**) have no Tf signals, as the Tf was completely expelled from cells. Scale bars: 20 μm.

at the cell periphery (Figure 5F). The labeling of lysosomal acid hydrolase cathepsin D was not particularly enriched in the GFP+ compartments (data not shown). These results together suggest that the R135L/GFPv-arr complexes induced the formation of hybrid organelles that contained the contents of the early, recycling, and late endosomes, and little or no lysosomal degradation activity occurred.

To assess the functional consequences of the changes in the endosomal organizations of cells that expressed R135L/GFPv-arr, we measured receptor-mediated endocytosis in these cells by use of Tf and LDL as probes for the recycling and lysosomally directed pathways, respectively. Both events have been well mapped out (8), and we have shown that HEK cells follow an endocytic trafficking scheme similar to that of other cell types (25). To examine Tf uptake, R135L/GFPv-arr–transfected cells were incubated with Alexa 594–Tf at 37°C for various time points before the cells were fixed for visualization. Within 5 minutes, Tf was found in the early endosomes throughout the untransfected cells (Figure 6, A and B). In contrast, very little or no Tf was detected in the transfected cells at this time point (Figure 6, A and B), which indicated that the efficiency of TfR-mediated Tf uptake was significantly reduced in cells that overexpressed R135L/GFPv-arr. After 2 hours of loading, Tf reached a steady-state occupancy of the early-endosome and the recycling endosomes in the untransfected control cells (Figure 6, E and F). In contrast, the internalized Tf was predominantly concentrated in the GFP+ perinuclear structures in transfected cells at this time point (Figure 6, E and F). We examined the recycling of Tf by incubating transfected cells with Alexa 594–Tf for 2 hours at 37°C and then chasing for 30 minutes. As expected (8), almost all the internalized Tf was recycled into the medium, and essentially no Tf was detectable in untransfected cells (Figure 6, I and J). In contrast, the Tf internalized and accumulated in the GFP+ compartments did not recycle and remained in these structures (Figure 6, I and J). These kinds of defects in endocytosis and recycling of Tf and LDL were not detected in cells cotransfected with WT rhodopsin and GFPv-arr (Figure 6, C and D, G and H, and K and L) or in cells singly transfected with R135L or GFPv-arr (data not shown).

Like Tf uptake, the uptake of 3,3′-diotadecylindocarbocyanine-LDL (DiI-LDL) was also reduced in cells that overexpressed R135L/GFPv-arr. As seen in Figures 6, M and N, a significantly lower level of DiI-LDL was seen in the transfected cells compared with the neighboring untransfected cells, after a 2-minute uptake and a 28-minute chase. In contrast, internalized LDL levels were indistinguishable between the control cells and WT rhodopsin/GFPv-arr–transfected cells (Figure 6, O and P) or cells singly transfected with R135L or GFPv-arr (data not shown). The severity of defects in the endocytic pathways of Tf and LDL generally appeared to be inversely proportional to the levels of intracellular accumulated R135L/GFPv-arr complexes. These results together suggested that the complex formation between R135L and v-arr is the key element that interfered with the dynamic interactions between distinct endocytic compartments as well as with the flow of the endocytic pathway.

Discussion

Novel class RP mutant rhodopsin-class III. Arg135 mutations in rhodopsin cause an aggressive form of RP. Patients with an Arg135 mutation usually experienced much faster progression to blindness than do patients who carry most other rhodopsin mutations: almost all young patients (under 20 years of age) examined exhibited substantial visual field loss and rod function impairment (26–29). The discernible difference in the pattern of retinal dysfunction of RP patients who carry Arg135 rhodopsin mutations is correlated with unique biochemical and cellular defects in the mutant proteins. At the present time, no typical class I or class II mutant rhodopsins tested share the same cellular defects as the Arg135 mutants. Arg135 mutations have been previously grouped as class IIb (an atypical form of class II mutations) (4, 5). However, no additional class IIb RP mutant rhodopsins (e.g., G106R, L152R, or C167R) (5) tested displayed similar phenotype (unpublished data). We propose that the Arg135 mutations are more likely to represent a novel class of RP rhodopsin mutations, which we call class III. In this regard, one other RP mutant rhodopsin of interest, K296E, has characteristics different from the typical class I and class II mutants. K296E activated transducin in the absence of chromophore (1) and also showed increased binding to v-arr (22, 30). Our unpublished results showed that K296E itself, unlike the Arg135 mutants, was primarily targeted to the PM but not the endocytic/lysosomal compartments. In addition, although the K296E mutant has some ability to recruit GFPv-arr to the PM, no intracellular vesicular structures that contain either molecule were detected in the cells cotransfected K296E and GFPv-arr (Chuang and Sung, unpublished data). The classification of K296E needs further analysis.

The importance of Arg135 residue for the proper opsin conformation has been indicated by a number of in vitro biochemical studies. Glu134/Arg135 residues were shown to be involved in transducin binding (31). All three RP Arg135 mutants failed to activate transducin in the presence 11-*cis* retinal (2), yet, bound to arrestin and RK in the absence of chromophore (10). Because human Arg135 mutant rhodopsins exhibited poor ability to bind to 11-*cis* retinal (4, 5), these mutants may primarily exist as apoproteins in vivo, similar to those expressed in the heterologous expression system. Although the 11-*cis* retinal chromophore may possibly assist the folding of Arg135 mutant proteins in rod outer segments, the high-affinity interaction between the Arg135 opsin apoprotein and v-arr is likely to allow complex formation shortly after protein synthesis and persist in the photoreceptor cell bodies. The PM and intracellular vacuole–like v-arr distributions in the R135L transfected rods strongly supported this hypothesis. The mutant rhodopsins were delivered postnatally in our ectopic retina expression system. We theorize that malfunction caused by the mistrafficked v-arr and rhodopsin could take place as soon as these proteins are expressed during the retinal development (32–34).

The various compartments along the endocytic pathway are generally considered to be distinct entities, each with a different pH, even though their contents are highly interchangeable through dynamic fusion, budding, or fission events (9). Our results suggest that stable complexes formed between Arg135 mutant and v-arr disrupt the dynamic interplay between the endocytic compartments and mix various endosomal compartments into a single compartment. Because endocytic processes are essential for nutrient uptake, iron transport, and surface signaling deactivation, one can imagine that a dysfunction in these activities could cause an imbalance in iron levels, nutrient levels, or both, which could subsequently lead to photoreceptor pathology. Indeed, previous studies have observed photoreceptor death caused by either a lack of iron (35) or an excess of iron (36, 37). The importance of iron-mediated biological functions in photoreceptors is further supported by the abundance of iron-binding proteins Tf and ferritin

in photoreceptors (38, 39). In fact, gene-profiling studies indicate that these two molecules are among the 10 most highly expressed genes in retinas (40). The specialized endocytic activity that takes place in rod synapses may also be affected in photoreceptors that carry Arg135 mutant rhodopsin. The endocytic compartment/activity alteration is very likely to lead to the structural and function damage of lysosomes. Although WT rhodopsins are normally transported to the outer segments and degraded through phagocytosis in the retinal pigment cells, abnormally internalized Arg135 rhodopsin protein complexes may significantly elevate the metabolic demands for proteolytic digestion of rod cell bodies. Inefficient proteolysis digestion has been proposed to be one major problem for the retinal pigment epithelial cell pathology in various macular degenerative diseases (41, 42).

A wealth of evidence has suggested that signal transduction could take place on endosomes (43). Many signaling pathways are induced by the recruitment of signaling molecules, such as MAP kinases and Src, via the scaffolding ability of β-arrestins. An assessment of the scaffolding ability of v-arr and its involvement in photoreceptor cell death would be of great interest.

The Arg135 residue is highly conserved among GPCR family members (44). Mutation of an equivalent Arg residue (R137H) in the vasopressin receptor is associated with nephrogenic diabetes insipidus (45). Consistent with this report, the vasopressin R137H mutation causes constitutive internalization and high-affinity binding to β-arrestin (46). An investigation of the involvement of endocytic defects in the pathogenesis of other diseases caused by GPCR mutations analogous to Arg135 would be of interest. Unraveling the molecular mechanisms that cause the fusion/aggregation of endosomal structures may provide insight into the development of therapeutic treatments for diseases of this type.

Physiological relevance of the rhodopsin endocytosis. Although arrestin-mediated endocytosis is an essential mechanism for most of GPCR desensitization, endocytosis has not been described as a pathway to shut off the phototransduction in rod outer segments. This finding was consistent with the lack of morphologically characteristic endocytic compartments in the outer segments. On the other hand, both endocytic compartments and activity have been described in the rod inner segments (47–49). Given our data that RK-phosphorylated WT rhodopsin may be sequestered into cells and bound to v-arr, we can speculate that the endocytic activity may also be used to remove superfluous photoactivated rhodopsin in rod inner segment/cell body under the pathological condition (e.g., excess light). In fact, light stimulus elevated the numbers of endocytic membranous profiles as well as the rhodopsin accumulation in the membranous vacuoles in the rod cell bodies (49, 50). This finding is a significant conceptual advance in regard to how rhodopsin protein is removed from the cell; it was previously thought to be removed exclusively by phagocytosis by retinal pigment epithelial cells. The stable rhodopsin–v-arr complexes accumulated in the endocytic compartments have been suggested to be the root cause of the light-induced, phototransduction-independent photoreceptor cell death in fly (6, 7). An examination of whether the rhodopsin sequestered in the cell bodies plays any role in the bright light–induced photoreceptor apoptosis in mammals that is also known to be mediated through a G-protein independent pathway would be of interest (51).

Novel animal model for RP study. At the present time, essentially no photoreceptor cell culture system can be used to systemically examine the molecular defects of various RP disease proteins. In the present paper, we demonstrate for the first time that an in vivo retinal transfection system can reproduce the results of previous transgenic studies, which suggests that this technique could become an invaluable means to model diseased rods.

Methods

Tissue culture expression. Expression vectors that encode the human WT and mutant rhodopsins (R135L, R135G, R135W, P23H, and Q344ter) in PRK-5 were described (4, 5). cDNA of bovine v-arr was RT-PCR amplified from bovine retinal RNA and fused to the C-terminus of GFP in the pEGFP-C1 vector (BD Biosciences, Palo Alto, California, USA). RK expression vector was courtesy of C.-K. Chen (University of Utah, Salt Lake City, Utah, USA) (52). Automated DNA sequencing was carried out to confirm the lack of spurious mutations. Transfection of HEK 293T cells (total 0.5–1 μg per 35-mm dish, 1:1 ratio for multiple plasmids) was performed by application of Lipofectamine 2000 (Invitrogen, Rockville, Maryland, USA) or a standard calcium phosphate method.

Immunocytochemistry of HEK cells. After transfection for 18 to 24 hours, cells grown on gelatin-coated cover slips were fixed with 4% paraformaldehyde (PFA) and permeabilized with 0.04% saponin and 1% BSA that contained PBS-C/M (0.2 mM $CaCl_2$ and 2 mM $MgCl_2$) for 30 minutes at room temperature before the Ab incubation. Primary antibodies used were anti–rhodopsin N-terminus B6-30 mAb (P. Hargrave, University of Florida, Gainesville, Florida, USA), EEA1 mAb (Transduction Laboratory, Lexington, Kentucky, USA), LAMP1 mAb (AC17; Enrique Rodriguez-Boulan, Weill Medical College of Cornell University, New York, New York, USA), and TfR mAb (H68.4; Zymed, South San Francisco, California, USA). Alexa 594– and Alexa 488–conjugated secondary antibodies were obtained from Molecular Probes (Eugene, Oregon, USA). All samples were mounted with Vectashield mounting medium that contained DAPI (Vector Laboratory, Burlingame, California, USA) and analyzed by Leica TCS SP2 spectral confocal system (Nussloch, Germany). The acousto-optical beam-splitter system and sequential image recording were used for image collection. The excitation wavelengths used were 488 nm and 543 nm for detection of Alexa 488 dye/GFP and Alexa 594 dye, respectively. The excitation intensities and spectral detection windows were systematically adjusted to optimize signals and avoid cross talk between channels. The absence of cross talk was routinely confirmed by single-channel excitation and dual-channel recording before the data collection. Twelve-bit images of single confocal sections (0.6 μm) were processed by Adobe Photoshop (San Jose, California, USA).

Whole-cell phosphorylation, immunoprecipitation, and Western blotting. For metabolic labeling, HEK cells were starved in phosphate-free DMEM (Invitrogen) for 30 minutes, labeled for 2 hours in the same medium that contained [^{32}P]orthophosphate (1 mCi/ml; PerkinElmer, Wellesley, Massachusetts, USA), and harvested for immunoprecipitation. Immunoprecipitation was carried out as described (4) by use of mAb B6-30. Western blot assays were carried out by the standard ECL method that utilized either mAb B6-30 or anti–GFP rabbit Ab (Molecular Probes).

Retinal transfection. DNA fragments that encoded human WT, Q344ter, and R135L rhodopsins were inserted into the pCAGIG vector (a chicken actin promoter fused with IRES followed by the GFP coding sequence; courtesy of C.L. Cepko (Harvard Medical School, Boston, Massachusetts, USA). The resulting pCAG-rhodopsin-IRES-GFP expression constructs (3 μg/ml in TE) were injected into the subretinal space of neonatal Sprague-Dawley

rats, followed by electroporation by tweezer-type electrodes (BTX, Hawthorne, New York, USA), which were placed across the eyes so that the cathode faced to sclera and the anode faced the cornea (Figure 4A). Five 100-V pulses of 50-millisecond duration and 950-millisecond resting interval were given (20). The injected eyes were enucleated at postnatal day 21 to 30 and fixed by 4% PFA. GFP-positive retinas were identified under epifluorescent microscope, embedded in 5% low-melting agarose, and vibratome sectioned (40 μm). Free-floating retinal sections were immunolabeled with either the human rhodopsin–specific mAb 3A6 (22) (courtesy of R. Molday, University of British Columbia, Vancouver, British Columbia, Canada), rabbit anti-Q344ter Ab (23), or rabbit anti–v-arr Ab (courtesy of I. Gary, National Institutes of Health, Bethesda, Maryland, USA), followed by Alexa 594–conjugated secondary antibodies. All samples were analyzed by Leica TCS SP2 spectral confocal system as described above. At least three animals were examined for each experiment. All methods that involved live animals were approved by the Weill Medical College of Cornell University Institutional Animal Care and Use Committee.

Endocytosis assays. Purified B6-30 IgG (10 μg/ml) was incubated for 1 hour at 4°C with live, transfected cells in serum-free DMEM supplemented with 0.5% BSA. Cells were washed in PBSC/M three times and chased in 10% FBS that contained DMEM for an additional 1 hour. Cells were then fixed/permeabilized and incubated with Alexa 594–conjugated anti-mouse Ab for visualization.

The uptake and recycling of Tf in HEK cells were measured as described (25). Briefly, for uptake experiments, cells were loaded with Alexa 594–Tf (3 μg/ml; Molecular Probes) in serum-free medium for 5 or 120 minutes at 37°C. Cells were then placed on ice, washed with mild acidic buffer for 2 minutes to remove surface bound Tf. Cells were then rinsed with PBSC/M and fixed in 4% PFA for visualization. In some experiments, Tf was loaded for 2 minutes and chased for 28 minutes to visualize the recycling endosomes (8). For recycling, cells were incubated with Alexa 594–Tf for 2 hours at 37°C and then chased for an additional 30-minute incubation at 37°C before fixation. To study the lysosomally directed endocytic pathway, DiI-labeled LDL (20 μg/ml; Molecular Probes) was loaded at 37°C for 2 minutes and chased for 28 minutes to label the late endosomes and late lysosomes (53). To label the late endosomes and lysosomes, cells were incubated with rhodamine-conjugated dextran (70 kDa; Molecular Probes) for 2 hours before fixation (53).

Acknowledgments

We thank Fuo-Ku Chu for technical help, our colleagues for reagents, and Timothy E. McGraw, Francis S. Lee, Hui Sun, and members of C.-H. Sung's laboratory for comments on the manuscript. We thank T. Matsuda and C.L. Cepko for sharing the in vivo electroporation technique before their publication and S. Anderson for allowing the use of the gene pulser. This work was supported by The Dolley Green Special Scholar Award and The Lew R. Waserman Merit Award (Research to Prevent Blindness), the Irma T. Hirschl Charitable Trust, and an NIH grant to C.-H. Sung (NIH-EY11307).

Received for publication January 22, 2004, and accepted in revised form May 11, 2004.

Address correspondence to: Ching-Hwa Sung, The Margaret M. Dyson Vision Research Institute, Weill Medical College of Cornell University, 1300 York Avenue, New York, New York 10021, USA. Phone: (212) 746-2291; Fax: (212) 746-6670; E-mail: chsung@mail.med.cornell.edu.

1. Robinson, P.R., Cohen, G.B., Zhukovsky, E.A., and Oprian, D.D. 1992. Constitutively active mutants of rhodopsin. *Neuron.* **9**:719–725.
2. Min, K.C., Zvyaga, T.A., Cypess, A.M., and Sakmar, T.P. 1993. Characterization of mutant rhodopsins responsible for autosomal dominant retinitis pigmentosa. Mutations on the cytoplasmic surface affect transducin activation. *J. Biol. Chem.* **268**:9400–9404.
3. Franke, R.R., Sakmar, T.P., Graham, R.M., and Khorana, H.G. 1992. Structure and function in rhodopsin. Studies of the interaction between the rhodopsin cytoplasmic domain and transducin. *J. Biol. Chem.* **267**:14767–14774.
4. Sung, C.H., Schneider, B.G., Agarwal, N., Papermaster, D.S., and Nathans, J. 1991. Functional heterogeneity of mutant rhodopsins responsible for autosomal dominant retinitis pigmentosa. *Proc. Natl. Acad. Sci. U. S. A.* **88**:8840–8844.
5. Sung, C.-H., Davenport, C.M., and Nathans, J. 1993. Rhodopsin mutations responsible for autosomal dominant retinitis pigmentosa. Clustering of functional classes along the polypeptide chain. *J. Biol. Chem.* **268**:26645–26649.
6. Kiselev, A., et al. 2000. A molecular pathway for light-dependent photoreceptor apoptosis in Drosophila. *Neuron.* **28**:139–152.
7. Alloway, P.G., Howard, L., and Dolph, P.J. 2000. The formation of stable rhodopsin-arrestin complexes induces apoptosis and photoreceptor cell degeneration. *Neuron.* **28**:129–138.
8. McGraw, T.E., and Maxfield, F.R. 1991. *Internalization and sorting of macromolecules: endocytosis.* Springer-Verlag. Berlin, Germany. 11–41.
9. Gruenberg, J. 2001. The endocytic pathway: a mosaic of domains. *Nat. Rev. Mol. Cell Biol.* **2**:721–730.
10. Shi, W., et al. 1998. Rhodopsin arginine-135 mutants are phosphorylated by rhodopsin kinase and bind arrestin in the absence of 11-cis-retinal. *Biochemistry.* **37**:4869–4874.
11. Sung, C.-H., et al. 1991. Rhodopsin mutations in autosomal dominant retinitis pigmentosa. *Proc. Natl. Acad. Sci. U. S. A.* **88**:6481–6485.
12. Macke, J.P., et al. 1993. Identification of novel rhodopsin mutations responsible for retinitis pigmentosa: implications for the structure and function of rhodopsin. *Am. J. Hum. Genet.* **53**:80–89.
13. Dunn, K.W., McGraw, T.E., and Maxfield, F.R. 1989. Iterative fractionation of recycling receptors from lysosomally destined ligands in an early sorting endosome. *J. Cell Biol.* **109**:3303–3314.
14. Illing, M.E., Rajan, R.S., Bence, N.F., and Kopito, R.R. 2002. A rhodopsin mutant linked to autosomal dominant retinitis pigmentosa is prone to aggregate and interacts with the ubiquitin proteasome system. *J. Biol. Chem.* **277**:34150–34160.
15. Barak, L.S., Ferguson, S.S., Zhang, J., and Caron, M.G. 1997. A beta-arrestin/green fluorescent protein biosensor for detecting G protein-coupled receptor activation. *J. Biol. Chem.* **272**:27497–27500.
16. Ferrari, S.L., Behar, V., Chorev, M., Rosenblatt, M., and Bisello, A. 1999. Endocytosis of ligand-human parathyroid hormone receptor 1 complexes is protein kinase C-dependent and involves beta-arrestin 2. Real-time monitoring by fluorescence microscopy. *J. Biol. Chem.* **274**:29968–29975.
17. van Engeland, M., Ramaekers, F.C., Schutte, B., and Reutelingsperger, C.P. 1996. A novel assay to measure loss of plasma membrane asymmetry during apoptosis of adherent cells in culture. *Cytometry.* **24**:131–139.
18. Ghosh, R.N., Mallet, W.G., Soe, T.T., McGraw, T.E., and Maxfield, F.R. 1998. An endocytosed TGN38 chimeric protein is delivered to the TGN after trafficking through the endocytic recycling compartment in CHO cells. *J. Cell Biol.* **142**:923–936.
19. Waguri, S., et al. 2003. Visualization of TGN to endosome trafficking through fluorescently labeled MPR and AP-1 in living cells. *Mol. Biol. Cell.* **14**:142–155.
20. Matsuda, T., and Cepko, C.L. 2004. Electroporation and RNA interference in the rodent retina in vivo and in vitro. *Proc. Natl. Acad. Sci. U. S. A.* **101**:16–22.
21. Flannery, J.G., et al. 1997. Efficient photoreceptor-targeted gene expression in vivo by recombinant adeno-associated virus. *Proc. Natl. Acad. Sci. U. S. A.* **94**:6916–6921.
22. Li, T., Franson, W.K., Gordon, J.W., Berson, E.L., and Dryja, T.P. 1995. Constitutive activation of phototransduction by K296E opsin is not a cause of photoreceptor degeneration. *Proc. Natl. Acad. Sci. U. S. A.* **92**:3551–3555.
23. Sung, C.-H., Makino, C., Baylor, D., and Nathans, J. 1994. A rhodopsin gene mutation responsible for autosomal dominant retinitis pigmentosa results in a protein that is defective in localization to the photoreceptor outer segment. *J. Neurosci.* **14**:5818–5833.
24. Molday, R.S., and MacKenzie, D. 1983. Monoclonal antibody to rhodopsin: characterization, cross-reactivity and application as structural probes. *Biochemistry.* **22**:653–660.
25. Hu, Y., Chuang, J.Z., Xu, K., McGraw, T.E., and Sung, C.H. 2002. SARA, a FYVE domain protein, affects Rab5-mediated endocytosis. *J. Cell. Sci.* **115**:4755–4763.
26. Jacobson, S.G., Kemp, C.M., Sung, C.H., and Nathans, J. 1991. Retinal function and rhodopsin levels in autosomal dominant retinitis pigmentosa with rhodopsin mutations. *Am. J. Ophthalmol.* **112**:256–271.

27. Pannarale, M.R., et al. 1996. Autosomal-dominant retinitis pigmentosa associated with an Arg-135-Trp point mutation of the rhodopsin gene. Clinical features and longitudinal observations. *Ophthalmology.* **103**:1443–1452.
28. Ponjavic, V., Abrahamson, M., Andreasson, S., Ehinger, B., and Fex, G. 1997. Autosomal dominant retinitis pigmentosa with a rhodopsin mutation (Arg-135-Trp). Disease phenotype in a Swedish family. *Acta. Ophthalmol. Scand.* **75**:218–223.
29. Andreasson, S., Ehinger, B., Abrahamson, M., and Fex, G. 1992. A six-generation family with autosomal dominant retinitis pigmentosa and a rhodopsin gene mutation (arginine-135-leucine). *Ophthalmic. Paediatr. Genet.***13**:145–153.
30. Rim, J., and Oprian, D.D. 1995. Constitutive activation of opsin: interaction of mutants with rhodopsin kinase and arrestin. *Biochemistry.* **34**:11938–11945.
31. Franke, R.R., Konig, B., Sakmar, T.P., Khorana, H.G., and Hofmann, K.P. 1990. Rhodopsin mutants that bind but fail to activate transducin. *Science.* **250**:123–125.
32. Morrow, E.M., Belliveau, M.J., and Cepko, C.L. 1998. Two phases of rod photoreceptor differentiation during rat retinal development. *J. Neurosci.***18**:3738–3748.
33. O'Brien, K.M., Schulte, D., and Hendrickson, A.E. 2003. Expression of photoreceptor-associated molecules during human fetal eye development. *Mol. Vis.* **9**:401–409.
34. Ratto, G.M., Robinson, D.W., Yan, B., and McNaughton, P.A. 1991. Development of the light response in neonatal mammalian rods. *Nature.* **351**:654–657.
35. Lakhanpal, V., Schocket, S.S., and Jiji, R. 1984. Desferoxamine (Desferal)-induced toxic retinal pigmentary degeneration and presumed optic neuropathy. *Ophthalmology.* **91**:443–451.
36. Rapp, L.M., Wiegand, R.D., and Anderson, R.E. 1982. *Ferrous ion-mediated retinal degerantion: role of rod outer segment lipid peroxydation.* Academic Press. New York, New York, USA. 109–119.
37. Wang, Z.J., Lam, K.W., Lam, T.T., and Tso, M.O. 1998. Iron-induced apoptosis in the photoreceptor cells of rats. *Invest. Ophthalmol. Vis. Sci.* **39**:631–633.
38. Davis, A.A., and Hunt, R.C. 1993. Transferrin is made and bound by photoreceptor cells. *J. Cell. Physiol.* **156**:280–285.
39. Yefimova, M.G., et al. 2000. Iron, ferritin, transferrin, and transferrin receptor in the adult rat retina. *Invest. Ophthalmol. Vis. Sci.* **41**:2343–2351.
40. Sharon, D., Blackshaw, S., Cepko, C.L., and Dryja, T.P. 2002. Profile of the genes expressed in the human peripheral retina, macula, and retinal pigment epithelium determined through serial analysis of gene expression (SAGE). *Proc. Natl. Acad. Sci. U. S. A.* **99**:315–320.
41. Feeney-Burns, L., and Eldred, G.E. 1983. The fate of the phagosome: conversion to 'age pigment' and impact in human retinal pigment epithelium. *Trans. Ophthalmol. Soc. U. K.* **103**:416–421.
42. Katz, M.L., and Shanker, M.J. 1989. Development of lipofuscin-like fluorescence in the retinal pigment epithelium in response to protease inhibitor treatment. *Mech. Ageing Dev.* **49**:23–40.
43. McDonald, P.H., and Lefkowitz, R.J. 2001. Beta-arrestins: new roles in regulating heptahelical receptors' functions. *Cell. Signal.* **13**:683–689.
44. Sprobst, W.C., Synder, L.A., Schuster, D.I., Brosius, J., and Sealfon, S.C. 1992. *DNA Cell Biol.* **11**:1–20.
45. Rosenthal, W., Antaramian, A., Gilbert, S., and Birnbaumer, M. 1993. Nephrogenic diabetes insipidus. A V2 vasopressin receptor unable to stimulate adenylyl cyclase. *J. Biol. Chem.* **268**:13030–13033.
46. Barak, L.S., Oakley, R.H., Laporte, S.A., and Caron, M.G. 2001. Constitutive arrestin-mediated desensitization of a human vasopressin receptor mutant associated with nephrogenic diabetes insipidus. *Proc. Natl. Acad. Sci. U. S. A.* **98**:93–98.
47. Hollyfield, J.G., and Rayborn, M.E. 1987. Endocytosis in the inner segment of rod photoreceptors: analysis of *Xenopus laevis* retinas using horseradish peroxidase. *Exp. Eye Res.* **45**:703–719.
48. Cotter, J.R. 1989. Endocytosis of cationized ferritin by rat photoreceptors. *Neurosci. Lett.* **106**:65–70.
49. Wunderer, H., Picaud, S., and Franceschini, N. 1989. Selective illumination of single photoreceptors in the house fly retina: local membrane turnover and uptake of extracellular horseradish peroxidase (HRP) and lucifer yellow. *Cell Tissue Res.* **257**:565–576.
50. Reme, C.E., Wolfrum, U., Imsand, C., Hafezi, F., and Williams, T.P. 1999. Photoreceptor autophagy: effects of light history on number and opsin content of degradative vacuoles. *Invest. Ophthalmol. Vis. Sci.* **40**:2398–2404.
51. Hao, W., et al. 2002. Evidence for two apoptotic pathways in light-induced retinal degeneration. *Nat. Genet.* **32**:254–260.
52. Chen, C.K., Inglese, J., Lefkowitz, R.J., and Hurley, J.B. 1995. Ca(2+)-dependent interaction of recoverin with rhodopsin kinase. *J. Biol. Chem.* **270**:18060–18066.
53. Dunn, K.W., and Maxfield, F.R. 1992. Delivery of ligands from sorting endosomes to late endosomes occurs by maturation of sorting endosomes. *J. Cell Biol.* **117**:301–310.